# Convective Impact on the Global Lower Stratospheric Water Vapor Budget

**Rei Ueyama[1], Mark Schoeberl[3], Eric Jensen[2], Leonhard Pfister[1], Mijeong Park[4], and Ju-Mee Ryoo[1,3]**

[1]NASA Ames Research Center.

[2]NOAA.

[3]Science and Technology Corporation.

[4]National Center for Atmospheri Research.

Corresponding author: Rei Ueyama (rei.ueyama@nasa.gov)

**Key Points:**

- Convection moistens the global lower stratosphere by 0.3 ppmv with interannual variations of up to 0.1 ppmv in winter and summer 2006-2016.
- Convection moistens the lower stratosphere primarily via the detrainment of saturated air and ice into the tropical uppermost troposphere.
- Deep convective systems overshooting the tropopause have a minor effect on global lower stratospheric water vapor.

## Abstract

Water vapor in the stratosphere is primarily controlled by temperatures in the tropical upper troposphere and lower stratosphere. However, the direct impact of deep convection on the global lower stratospheric water vapor budget is still an actively debated issue. Two complementary modeling approaches are used to investigate the convective impact in boreal winter and summer. Backward trajectory model simulations coupled with a detailed treatment of cloud microphysical processes indicate that convection moistens the global lower stratosphere by approximately 0.3 ppmv (~10% increase) in boreal winter and summer 2010. The diurnal peak in convection is responsible for about half of the total convective moistening during boreal winter and nearly all of the convective moistening during boreal summer. Deep convective cloud tops overshooting the local tropopause have relatively minor effect on global lower stratospheric water vapor (~1% increase). A forward trajectory model coupled with a simplified cloud module is used to esimate the relative magnitude of the interannual variability of the convective impact during 2006-2016. Combing the results from the two models, we find that the convective impact on the global lower stratospheric water vapor during 2006-2016 is approximately 0.3 ppmv with year-to-year variations of up to 0.1 ppmv. The dominant mechanism of convective hydration of the lower stratosphere is via the detrainment of saturated air and ice into the tropical uppermost troposphere. Convection shifts the relative humidity distribution of subsaturated air parcels in the upper troposphere toward higher relative humidity values, thereby increasing the water vapor in the stratosphere.



## Plain Language Summary

Stratosphere is extremely dry, but small changes in the humidity of the stratosphere can have a big impact on Earth's climate. Water vapor in the stratosphere is primarily determined by temperatures in the tropical upper atmosphere (between the tropospheric and stratospheric layers), but deep convective clouds that rapidly transport humid air up to this region could potentially influence stratospheric water vapor as well. This study uses two complementary modeling approaches to estimate the overall impact of deep convection on global stratospheric humidity. We find that convection moistens the lower stratosphere by about 10% in boreal winters and summers with smaller (by about a third) year-to-year variations during the 2006-2016 period. The daytime peak in convection is responsible for about half of the total convective moistening during boreal winter and nearly all of the convective moistening during boreal summer. Deep convective cloud tops that penetrate into the lower stratosphere have a relatively small effect on stratospheric water vapor. Convection moistens the lower stratosphere primarily by transporting humid air laden with numerous ice crystals to the tropical uppermost troposphere, just below the stratosphere. Some of this humid air subsequently ascends into the stratosphere and ultimately increases the humidity of the lower stratosphere.


## 1 Introduction

Water vapor is an important greenhouse gas and exerts significant influence on the chemistry and radiative balance of the atmosphere (e.g., Anderson et al., 2012; Forster & Shine, 1999, 2002; Solomon et al., 2010). Tropospheric water vapor, for instance, amplifies the direct warming from carbon dioxide via a strong positive feedback mechanism (Schneider et al., 1999;

Sherwood et al., 2010). Brewer (1949) hypothesized that the dryness of the stratosphere could be explained by the existence of a global circulation in which air enters the stratosphere through the cold tropical tropopause where it is dehydrated to the ice saturation level, moves poleward, and descends back down to the troposphere in the extratropics. This large-scale circulation in the stratosphere is known as the Brewer-Dobson circulation (BDC). Yulaeva et al. (1994) later interpreted the relationship between low- and high-latitude temperature annual cycles observed in the lower stratosphere as a result of variations in the strength of the wave-driven BDC. The annual cycle in tropical tropopause temperature, with a minimum in boreal winter and a maximum in boreal summer, produces a 'tape recorder' signal in time-height section of zonal-mean water vapor mixing ratios as seen by satellites (Fueglistaler et al., 2005; Mote et al., 1996; Schoeberl et al., 2008). These and other studies (see Fueglistaler et al., 2009 and references therein) highlight the importance of the strength of the tropical upwelling in the BDC in modulating the cold-point tropical tropopause temperature (Holton et al., 1995) which then controls the stratospheric water vapor budget as described further below.

Despite its very low concentration, stratospheric water vapor affects the chemistry (Anderson et al., 2012; Dvortsov & Solomon, 2001; Kiehl & Solomon, 1986), radiative forcing (Forster & Shine, 1999; Li & Newman, 2020; Solomon et al., 2010), and atmospheric circulation (Maycock et al., 2013). It also produces various feedbacks on the climate system (Banerjee et al., 2019; Dessler et al., 2013; Huang et al. 2020). Because of its significant role on climate, long-term observations of stratospheric water vapor have been made using balloons (Hurst et al., 2016) and various satellite instruments such as Aura Microwave Limb Sounder (MLS: Livesey et al., 2020). These measurements have been useful for monitoring long-term changes and variability in stratospheric humidty, and allowing investigations of processes that influence stratospheric water vapor.

As noted earlier, it is generally well understood that the stratospheric water vapor budget is, to first order, controlled by the slow large-scale ascent through the cold tropical tropopause (Fueglistaler et al., 2005; Gettelman et al., 2002; Hatsushika & Yamazaki, 2003; Holton & Gettelman, 2001; Mote et al., 1996; Randel & Jensen 2013; Randel & Park, 2019). Processes associated with atmospheric waves and convection also play a role in the dehydration of air entering the stratosphere through the tropical tropopause layer (TTL). These include dehydration driven by the cooling phase of gravity, Kelvin and Rossby waves (Boehm & Verlinde, 2000; Chang & L'Ecuyer, 2020; Dinh et al., 2016; Fujiwara et al., 2009; Garrett et al., 2004; Immler et al., 2008; Jensen & Pfister, 2004; Kim et al., 2016; Potter & Holton, 1995; Reinares Martinez et al., 2021; Schoeberl et al., 2015, 2016; Virts et al., 2010) and by the adiabatic cooling of air within deep convective overshooting cloud tops (Danielsen, 1982; Garrett et al., 2004, 2006; Gasparini et al., 2019; Hartmann et al., 2001; Kim et al., 2018; Potter & Holton, 1995; Robinson & Sherwood, 2006; Sherwood & Dessler, 2000; Sherwood et al., 2003). Additionally, cloud (microphysical, dynamical and radiative) processes and the direct injection of water vapor and ice by deep convection may also increase stratospheric water vapor (Corti et al., 2008; Danielsen 1993; Jensen & Pfister, 2004; Kelly et al., 1993; Kritz et al., 1993; Nielsen et al., 2007; Pfister et al., 1993; Schoeberl et al., 2014, 2016, 2018; Ueyama et al., 2015, 2018, 2020).

The climatological mean distribution of lower stratospheric (83 hPa) water vapor obtained from the Aura MLS measurements in boreal winter and summer is shown in Figure 1. In boreal winter, there is a distinct minimum in water vapor mixing ratios over the western tropical Pacific, roughly coincident with the region of minimum tropopause temperatures. In

contrast, there is no obvious relationship between lower stratospheric water vapor and temperature fields in boreal summer. Rather, enhanced water vapor over the Asian summer monsoon region appears to be collocated with a region of deep convective activity. The high water vapor mixing ratios in the extratropics are due to the transport of moist air associated with methane photolysis at higher altitudes in the stratosphere (Wofsy et al., 1972).

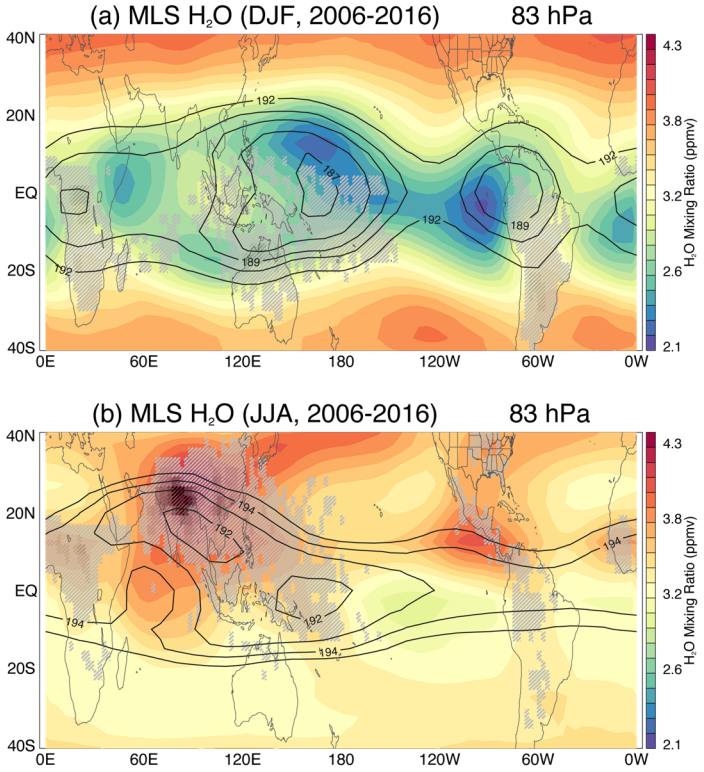


Figure 1: Climatological (2006-16) (a) winter (Dec-Jan-Feb) and (b) summer (Jun-Jul-Aug) mean water vapor mixing ratios (colored shading) in the lower stratosphere based on MLS observations at the 83 hPa level. The water vapor field is superimposed with gray shadings representing the occurrence frequency of deep convective cloud tops (>380 K) during the respective seasons: light to dark shading represents low to high cloud occurrence frequency. Also shown are contours of the cold-point tropopause temperature climatology from the Global Positioning System (GPS) radio occultation data for the same time period (see Randel & Wu, 2015).

The role of deep convection as a source of stratospheric water vapor has been explored over decades (Adler & Mack, 1986; Avery et al., 2017; Corti et al., 2009; Danielsen, 1993; Dessler et al., 2016; Kelly et al., 1993; Nielsen et al., 2007; Schoeberl et al., 2014, 2018, 2019; Smith et al., 2017; Wang et al., 2019). There is evidence of the direct injection of ice crystals (and subsequent sublimation) in the lowermost stratosphere by deep convection overshooting the tropopause, particularly over the midlatitude North American monsoon region (Schwartz et al., 2013; Smith et al., 2017). However, the impact of tropopause-overshooting convection on the global stratospheric water vapor budget is unclear (e.g., Jensen et al., 2020). In the current climate, only a small fraction of convective systems penetrate high enough into the stratosphere to have a significant impact.

The detrainment of ice into the tropical uppermost troposphere could potentially hydrate the lower stratosphere, if the detrained ice and the convectively-influenced air parcel do not encounter supersaturated (with respect to ice) air during their ascent into the stratosphere. Trajectory studies indicate that most parcels entering the tropical stratosphere have been dehydrated by in situ cloud formation, limiting the convective hydration of the tropical uppermost troposphere to at most ~0.5 ppmv (Schoeberl et al., 2018; Ueyama et al., 2015, 2018). These studies also show that the impact of convectively-detrained ice crystals on the humidity of the upper troposphere is relatively small compared to the total convective impact (Schoeberl et al., 2014; Ueyama et al., 2020).

We also note that convection can indirectly influence the lower stratospheric water vapor budget by lowering the temperatures in the upper troposphere and lower stratosphere (UTLS). For example, Randel et al. (2015) found that strong convection leads to relatively cooler and thus dry stratosphere (and vice versa) over the summer monsoon regions just above the altitude of maximum convection. This observation is consistent with an earlier model result by Salby & Callaghan (2004) that demonstrated a cooling and elevation of the tropical tropopause induced by an intensification or deepening of convection.

While aforementioned studies suggest that deep convective sources of stratospheric water vapor are generally small, a quantitative assessment of convective impact is missing on global and regional scales. Furthermore, detailed investigation of the year-to-year variability of the convective impact is still lacking. Eulerian models can include some important feedback effects, but subgrid scale processes that impact stratospheric water vapor (including convection, gravity waves, and cloud processes) are often poorly represented. Lagrangian models that resolve the various subgrid scale processes are better suited to investigate the relative importance of these processes on the stratospheric water vapor budget. Our understanding of the sensitivities of stratospheric water vapor to convective impact is limited in part due to uncertainties in the height of the convective cloud tops as well as its diurnal variability. Therefore, time-resolved, observation-based estimates of convection are critical for an accurate assessment of the convective impact. Since convective activity is likely to change in a warmer climate (e.g., Chou & Chen, 2010; Held & Soden, 2006; Romps 2011; Tan et al., 2015), such a study is necessary to improve simulations of UTLS processes in global climate models.

In this study, we address the following science questions:

1. What is the impact of convection on the global lower stratospheric water vapor budget?
2. How does the convective impact vary regionally and interannually?
3. What is the dominant mechanism of convective hydration or dehydration?

We first use the backward trajectory model with a detailed cloud microphysics scheme to investigate the convective impact on global lower stratospheric humidity during boreal winter and summer 2010. We then use the forward trajectory model to quantify the interannual variability of the convective impact. The results of this study will provide valuable insights on how future changes in convection may influence the global stratospheric water vapor budget, which then feedback on the climate system and ultimately affect Earth's climate.

## 2 Data and Methodology

### 2.1 Satellite observation of lower stratospheric water vapor

One of the main goals of this work is to understand the long-term measurements of lower stratospheric (83 hPa) water vapor from the Microwave Limb Sounder (MLS) onboard the Aura satellite. The MLS instrument scans Earth's limb and retrieves approximately 3,500 profiles each day between 82ºS and 82ºN latitudes. Level 2 version 5 water vapor retrievals (Lambert et al., 2020; Livesey et al., 2020) are analyzed in this study. This version corrects for the temporal calibration drift that appeared around 2010 (Hurst et al., 2016) as well as the dry bias (~20%) below the tropopause; these changes resulted in a 5-10% reduction in stratospheric water vapor compared to the previous versions (Lambert et al., 2015, 2020; Livesey et al., 2021). The 83-hPa water vapor precision and accuracy are both 7%. The data are screened for quality based on criteria indicated in Livesey et al. (2020).

We focus on boreal winter and summer 2010 for comparison between simulated and observed water vapor fields at the 83 hPa level. Year 2010 was chosen because lower stratospheric water vapor enhancements over the two monsoon regions were particularly clear that summer and resembled those of climatology (Fig. 1). Winter 2010 is calculated as the average from December 2009 through February 2010, while summer 2010 is calculated as the average from June through August 2010. We also examine the interannual variations over the 2006-2016 time period. The long-term (2006-2016) seasonal mean water vapor fields shown in Figure 1 are constructed by averaging 7-day averaged data on a 5º latitude x 5º longitude grid over three months.

### 2.2 Satellite-derived global convective cloud top altitudes

Current global models have difficulty simulating deep convection and tend to substantially underestimate the occurrence of deep convective clouds penetrating the TTL (e.g., Schoeberl et al., 2018). In order to accurately quantify the convective impact on the lower stratosphere on a global scale, we require observation-based estimates of the global convective cloud top altitudes at high temporal and spatial resolutions. We use the methodology described in previous studies (Bergman et al., 2012; Pfister et al., 2001; Schoeberl et al., 2018; Ueyama et al., 2015, 2018, 2020) with some modifications. Based on precipitation measurements from Tropical Rainfall Measuring Mission and Global Precipitation Measurement (GPM; Hao et al., 2014), convective regions are first identified by searching for rainfall rates exceeding a threshold value of 0.9 mm $h^{-1}$ over land and 1.5 mm $h^{-1}$ over ocean. These rainfall threholds are determined such that the resulting occurrence frequencies of deep convective cloud top heights (e.g., Figure 1) statiscally agree with those based on combined CloudSat and Cloud-Aerosol Lidar with Orthogonal Polarization (CALIOP) observations. A cloud top altitude is estimated by matching the infrared brightness temperature within a given convective region to the local temperature profile. To account for the observed cooling effect of convection near the tropopause (Chae et al., 2011; Selkirk, 1993; Sherwood et al., 2003), the analysis temperatures are modified above the analysis tropopause by calculating a profile that is a mixture of (70%) tropopause air and (30%) environmental air.

The climatological mean distribution of deep convection (i.e., cloud tops > 380 K) shows enhanced activity over distinct regions (Fig. 1), most frequently over land. In boreal winter, deep convective clouds are primarily observed over northern Australia, tropical Africa and South America. They also occur relatively frequently over the tropical western Pacific. In boreal

summer, deep convective activity dominates over the Asian monsoon land region as well as over tropical Africa to a lesser extent. Ueyama et al. (2018) used these satellite-derived convective cloud top heights to investigate the impact of convection on the uppermost troposphere during boreal summer. They found that convection was the primary driver of the enhancement in upper tropospheric water vapor over the Asian monsoon region.

Deep convection over the North American monsoon region occurs relatively infrequently based on this dataset. For the purpose of a case study to quantify the sensitivity of lower stratospheric water vapor to convective cloud top heights, we correct for the underestimated cloud tops over North America by modifying the convective cloud top potential temperatures over the northern midlatitudes in year 2010 when lower stratospheric water vapor was particularly enhanced over the North American monsoon region. Instead of assuming that convection overshooting the tropopause mixes with 70% tropospheric and 30% stratospheric air, we use a 50-50 mixture in northern midlatitudes. This modification has the effect of warming the plume and raising the altitude and potential temperature of the cloud tops. The resulting global distribution of deep convective clouds in 2010 resembles the climatological mean distribution shown in Figure 1, except for a five fold increase in the maximum occurrence of deep convective cloud tops (above 380 K potential temperature level) over the continental U.S. during summer (not shown).

To permit comparisons with previous studies utilizing this cloud top dataset (e.g., Schoeberl et al., 2018; Ueyama et al., 2015), we have used the original (unmodified) version for model comparison and for the investigation of the interannual variability of the convective impact. Figure 2a shows the interannual variability of global deep convective activity in boreal winters and summers from 2006 through 2016. Various modes of climate variability such as the El Niño Southern Oscillation (ENSO) presumably affect the global convective activity. Deep convection was relatively active in year 2010, which began with a warm ENSO winter followed by a slightly cold ENSO summer. The simulated lower stratospheric water vapor fields during boreal winter and summer 2010 are evaluated in Section 3.1. It is evident from Figure 2b that deep convective activity is particularly large over the Asian monsoon region in boreal summer, although convective activity over the North American monsoon region exhibits similar year-to-year variability with smaller magnitude. We will explore the relationship between year-to-year variations in deep convection and estimated convective impact on the UTLS using the forward trajectory model in Section 3.2.

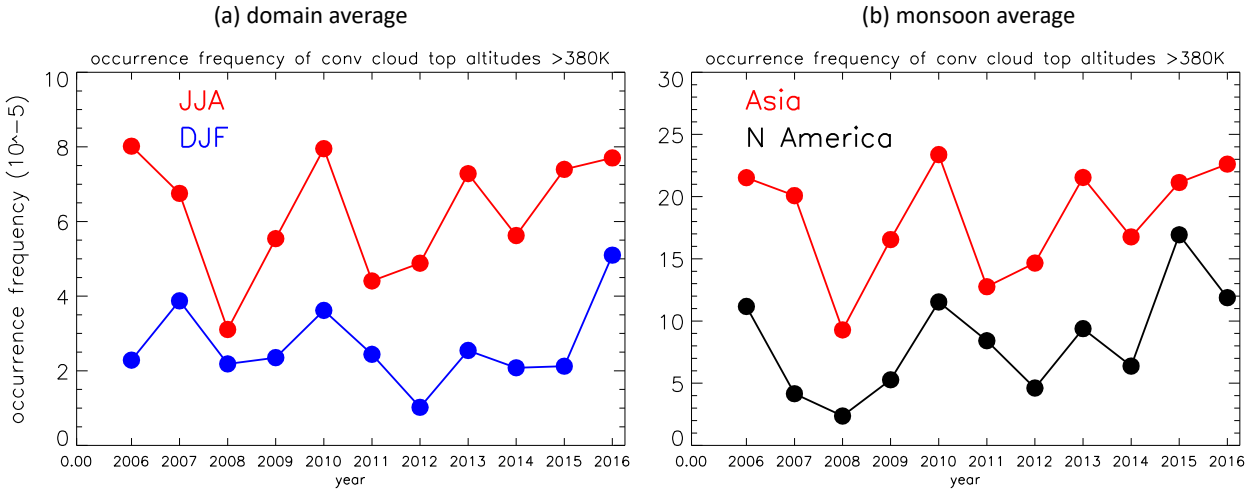

Figure 2: (a) Time series of the occurrence frequency of deep convection (cloud tops above the 380 K potential temperature level) over 30ºS-30ºN in winter and 20ºS-50ºN in summer during 2006-16. (b) As in (a) but for the Asian (red; 0-45ºN, 0-180ºE) and North American (black; 0-45ºN, 0-180ºW) monsoon regions during summer. Occurrence frequencies over the North American monsoon region are multiplied by a factor of 10. Occurrence frequency from December 2005 through February 2006 is plotted as the winter 2006 value.

## 2.3 Model description

**Table 1:** Model configuration and characteristics of the backward and forward trajectory modeling approaches used in this study.

| | Backward trajectory model | Forward trajectory model |
|---|---|---|
| **Parcel launch method** | • 2º lat x 2º lon grid within a domain (30ºS-30ºN for winter, 20ºS-50ºN for summer)<br>• At 390 K potential temperature level<br>• At a given date (21 Feb 2010 for winter, 22 Aug 2010 for summer) | • At the tops of convective clouds within the 40ºS-40ºN domain<br>• Continuously every 6 hours starting in year 2000 |
| **Trajectory length** | 75 days | Variable |
| **Analysis (T, U, V) data** | ERA5 | MERRA-2 |
| **Diabatic heating rates** | satellite-based heating rates[1] | MERRA-2 |
| **Convection scheme** | Satellite-based convective cloud top heights[2] | Satellite-based convective cloud top heights[2] |
| **Gravity wave scheme** | Gravity wave spectra from lower stratospheric superpressure balloon measurements[3] | Gravity wave spectra from lower stratospheric superpressure balloon measurements[3] |
| **Cloud scheme** | One-dimensional column model where cloud microphysical processes such as nucleation, deposition growth, sedimentation, and sublimation are simulated in vertical space along each trajectory path. | Zero-dimensional cloud model that tracks the mean ice crystal numer density, mass, and size, as well as the water vapor mixing ratio. Sedimentation, deposition growth and sublimation are approximated. |
| **Advantages** | • Provides direct estimates of water vapor at the desired locations<br>• Provides information about source and history of air parcels | • Computational efficiency allows for good statistics from abundant parcel tracking.<br>• Provides continuous picture of the time evolution |

| | | |
|---|---|---|
| | • Detailed cloud microphysical model accounts for vertical redistribution of water by ice cloud processes. | |
| **Limitations** | • Does not correctly represent air parcel age distribution if the mean age exceeds the trajectory integration time<br>• Lack of mixing between parcels<br>• Assumes no vertical wind shear of the horizontal wind along the trajectories[4]<br>• Trajectories need to be sufficiently long for the parcels to traverse through the cold tropopause temperatures. | • Does not provide detailed information about air parcel origins and pathways<br>• Results influenced by parcel launch locations<br>• Lack of mixing between parcels<br>• Ice sedimentation loss rate calculation requires an assumption of the parcel (cloud) depth<br>• Cloud parameterization assumes monodispersed ice crystal size distribution. |

*Note*. See also descriptions in the following references for the backward (Jensen & Pfister, 2004; Ueyama et al., 2015, 2018, 2020) and forward (Schoeberl and Dessler, 2011; Schoeberl et al., 2014, 2016) trajectory model approaches. [1] 2B-FLXHR-LIDAR (L'Ecuyer et al., 2008; Henderson et al., 2013); [2] See Section 2.2; [3] See Schoeberl et al. (2017); [4] Applies to the curtain model approach used in this study.

### *2.3.1 Backward trajectory (BT) model approach*

The backward trajectory (BT) model approach generally follows the methodology of Ueyama et al. (2015, 2018, 2020) and is summarized in Table 1. We first calculate 75-day BTs from 2º latitude x 2º longitude grid points in a given domain at the 390 K potential temperature level. For the winter simulation, we initialize the BTs from 30ºS to 30ºN domain on 21 February 2010 going back in time to early December 2009. For the summer simulation, we initialize the BTs from 20ºS to 50ºN domain on 22 August 2010 going back to early June 2010. Trajectories are calculated using hourly horizontal wind data from the European Centre for Medium-range Weather Forecast reanalysis (ERA5; Hersbach et al., 2020). ERA5 data are available at 29 levels between 50 and 300 hPa levels with ~5 hPa resolution in the UTLS (e.g., 73, 78, 83, 89, 94, 191, 107 hPa). For the vertical motions of the parcels, we use a combined broadband flux and heating rate product of the CloudSat, Cloud-Aerosol Lidar and Infrared Pathfinder Satellite Observations (CALIPSO) and Moderate Resolution Imaging Spectroradiometer (MODIS) missions (2B-FLXHR-LIDAR: Henderson et al., 2013; L'Ecuyer et al., 2008). Due to the lack of global coverage of the satellite-based heating rates at high enough resolution, the data are averaged over a three-month period to compute seasonal means (December-January-February for winter, June-July-August for summer). Although there is large uncertainty associated with an individual trajectory pathway, the averaging over thousands of trajectories within a large domain captures the transport characteristics through the UTLS reasonably well (Bergman et al., 2012).

After the trajectories have been calculated, we extract vertical profiles (from the 350 to 430 K potential temperature levels) of ERA5 temperatures at each time step along each trajectory

path to generate time vs. height "curtains" of temperatures. Although the effect of high-frequency gravity waves on TTL humidity appears to be small (Fueglistaler & Baker, 2006; Schoeberl et al., 2014, 2015; Ueyama et al., 2015), gravity waves have been shown to affect cloud microphysical properties (Dinh et al., 2016; Jensen & Pfister, 2004) and increase the occurrence of in situ formed clouds due to their modulation of the cooling rates (Schoeberl et al., 2015, 2016; Ueyama et al., 2015). We therefore add the effects of these waves on the temperature curtains using the gravity wave spectra calculated from Project Loon's lower stratospheric superpressure balloon measurements (Schoeberl et al., 2017) similar to the climatological mean high-frequency gravity wave spectra described in Jensen & Pfister (2004).

The temperature curtains, along with curtains of heating rates, are used to drive the one-dimensional (column) cloud microphysical model in the next step. Specifically, the cloud model is initialized with the 7-day mean gridded MLS water vapor profile nearest to the parcel location at the earliest time of the trajectory (i.e., 75 days before the BT launch date). Cloud ice processes such as nucleation, deposition growth, sedimentation, and sublimation are then simulated in one-dimensional (vertical) space along each trajectory path (from the earliest to latest time in the forward direction). For example, homogeneous ice nucleation is triggered when the ice saturation mixing ratio exceeds a threshold of ~1.6 (Koop et al., 2000). We do not include heterogeneous ice nucleation processes (which are triggered at a lower supersaturation of ~1.3) since Ueyama et al. (2015) have shown that water vapor and clouds in the TTL are relatively insensitive to the heterogeneous freezing process.

Ice crystals formed after nucleation are assumed to be in thermal equilibrium with the ambient air. Thus, if an ice crystal encounters subsaturated or supersaturated air, it will sublimate or grow by deposition, respectively. In order to model the cloud evolution, the sizes and heights of thousands of individual ice crystals are tracked throughout their lifetime. Water vapor is treated in an Eulerian grid, and the water exchange between the vapor and condensed phases is computed at each time step. The vertical advection of water vapor and ice crystals (including sedimentation of ice) is diagnosed using the heating rate curtains. In this way, this column cloud microphysical model properly treats the vertical redistribution of water by clouds,.

The water and cloud evolution along the trajectory path can be affected by an encounter with a convective cloud. To diagnose the convective influence, we trace the BTs through time-varying global convective cloud top altitude fields (described in Section 2.2) to identify convective cloud encounters along each trajectory path. Whenever a trajectory intersects a convective cloud, the column model is saturated up to the cloud top potential temperature. Convection will hydrate the environment if the column is initially subsaturated, while it will dehydrate the environment if the column is initially supersaturated. In situ measurements near convection indicate frequent supersaturation in the tropical upper troposphere (e.g., Krämer et al., 2020), while overshooting convection into the lower stratosphere will most likely encounter dry, subsaturated air. Deep convection often deposits ice crystals near the cloud top to form anvil cirrus, but convectively-detrained ice crystals in aging anvils have a relatively minor impact on TTL humidity (Ueyama et al., 2020). To quanfity their impact on lower stratospheric humidity, monodispersed ice crystals of diameter 30 μm with an ice water content of 30 ppmv are added the column model up to the cloud top potential temperature, as in Ueyama et al. (2020). When comparing the simulated water vapor ratios to those of MLS observations, we apply the MLS averaging kernel on the simulated water vapor profiles on the final day (i.e., BT launch date) and compare the values at the 83 hPa level.

The BT method provides direct estimates of the water vapor at the desired locations, which in this case is the global lower stratosphere. The limitations of any BT method include the need to run separate sets of trajectories for each valid time and the lack of mixing between parcels. Inter-parcel mixing along the trajectories (which is ignored here) has been found to potentially increase the humidity of the lower stratosphere particularly around the subtropical jets in the summer hemispheres (Poshyvailo et al., 2018). The simulated water vapor mixing ratios are averaged over the 5º latitude x 5º longitude grid to crudely represent mixing of air parcels. Furthermore, the BT "curtain" approach assumes no vertical wind shear of the horizontal wind along the trajectories. The laminar structure of TTL cirrus clouds clearly suggests the presence of vertical wind shear in the UTLS region. However, given the relatively short lifetimes of wide-scale cirrus clouds on the order of 1-2 days (Jensen et al., 2011), the dehydration and rehydration effects of cloud processes on the water vapor profile appear to be relatively insensitive to vertical wind shear. Another drawback is that when ascent rates in the UTLS are relatively slow such as during summer, BTs need to be sufficiently long for the parcels to traverse through the cold temperatures near the tropopause. If a parcel does not descend far enough below the tropopause (in reverse time), clouds will not form along the trajectory (in forward time) and the initialized MLS water vapor mixing ratio propagates forward *unless* the parcel intersects with convection. Although only ~10% of the summertime parcels at the 390 K potential temperature level descend below the 370 K level in 75 days, nearly all of the parcels encounters convection and/or form clouds along the 75-day trajectories such that this should not be an issue for characterizing the global mean impact of convection.

### *2.3.2 Forward trajectory (FT) model approach*

The forward trajectory (FT) model approach follows the forward domain filling methodology of Schoeberl and Dessler (2011) and is compared to the BT model approach in Table 1. In previous studies, parcels in the FT model were released on a fixed latitude-by-longitude grid at a specified potential temperature surface (typically between 360 and 370 K) just above the level of zero tropical radiative heating; this ensures that the parcels ascend into the stratosphere rather than immediately descend back into the lower troposphere. In this study, about 40,000 parcels are continuously released every day at each convective cloud top above 330 K (~10 km) over the 40ºS to 40ºN latitude domain. This method is more consistent with the BT approach described in Section 2.3.1 where parcels in the lower stratosphere are tracked backwards in time and intercept convective clouds along their trajectories. The FT parcels are initialized with the climatological (2005-15) daily mean MLS water vapor mixing ratio at that location. At the end of each day, any parcels that have descended below the 340 K level are removed, as well as those parcels that have reached the model top at ~2500 K level (about 0.4 hPa or 55 km). The model reaches a quasi-steady state with ~500,000 parcels after several years of integration.

The FTs are calculated based on the Bowman trajectory model (Bowman, 1993; Bowman and Carrie, 2002) using six-hourly horizontal winds and diabatic heating rates from MERRA-2 (Gelaro et al., 2017). We use a simplified zero-dimensional cloud model that tracks the mean ice crystal numer density, mass, and size, as well as the water vapor mixing ratio (Fueglistaler & Baker, 2006; Schoeberl et al., 2014, 2016). Ice nucleation is triggered when the ice saturation ratio exceeds a threshold of 1.6, as in the BT approach. The number of ice nuclei depends on the cooling rate derived from Kärcher et al. (2006), which are modulated by the same high-frequency gravity wave spectra in the BT approach. The total ice mass is computed from the ice

volume mixing ratio and density of ice at the parcel temperature. Ice particle effective radius is then calculated by dividing the total ice mass by the number of particles, all of which are assumed to be spherical. The simplified cloud model calculates ice crystal growth by deposition based on temperature, saturation, and partical radius. It also simulates ice crystal loss by sedimentation where the sedimentiation loss rate is inversely proportional to the assumed parcel vertical dimension of 500 m based loosely on CALIOP observations. One of the important differences between the backward and forward trajectory model approaches is that the microphysical scheme of the BT model allows for the sublimation of falling hydrometeors (Table 1).

Similar to the convective incluence analysis of the BT parcels, convective encounters of FT parcels are identified by tracking the parcels through the time-varying, satellite-derived convective cloud top altitude field. At each convective encounter, the parcel is saturated (i.e., relative humidity is reset to 100%) and a small amount of ice is added. The number and size of convective ice crystals added are based on tropical convection observations of Frey et al. (2014; see their Table 1). The water vapor mixing ratios of parcels scattered over the lower stratospheric domain during the winter and summer months are averaged into fixed latitude-by-longitude grid and compared with seasonal mean MLS water vapor at the 83 hPa level. This averaging crudely simulates parcel mixing, as mentioned above.

The FT model approach has the advantage of providing a time series of the full three-dimensional water vapor field throughout the stratosphere from a single simulation. However, the FT model does not save the individual parcel paths like the BT model. Instead, the location and time of specific events (e.g., last dehydration event or tropopause crossing) are recorded. The two models are also configured to use different reanalysis fields (Table 1). The implications of these model differences are discussed in the next section.

# 3 Results

## 3.1 Winter and summer 2010

### *3.1.1 Model evaluation*

The 83-hPa water vapor fields in boreal winter and summer 2010 are simulated in the backward and forward trajectory models and evaluated against their corresponding MLS observations in Figures 3 and 4. The BT simulation is for a single day (due to computational limitations), whereas the MLS and FT model fields are for a seven day period.

The seven-day mean water vapor field centered on 21 February 2010 (i.e., 18-24 February 2010) exhibits significant spatial variability with regional-scale anomalies (Fig. 3a). The BT model does not place the water vapor anomalies in the exact location as observed by MLS partly because the simulated water vapor field is for a single day (Fig. 3c). The magnitude and location of the water vapor anomalies vary significantly on a weekly basis as well as from year to year (not shown). Also, even though the MLS averaging kernel is applied to the simulated water vapor profiles, the simulated profiles are based on BTs calculated from a single level (390 K) and thus may not capture relatively shallow water vapor features found in the observations above and below the BT launch level. Nonetheless, the large-scale pattern resembles that of observations with the driest regions over the deep tropics. The observed dryness of the southern tropics is underestimated in the BT model, yielding an overall moist bias

of the BT model in boreal winter (Fig. 3e). In contrast, the FT model exhibits an overall dry bias especially in the southern hemisphere (Figs. 3d and f). Despite these model differences, both models simulate minimum water vapor over equatorial South America, which coincides with the region of minimum cold-point tropopause temperature (Fig. 3b). Differences in the lower stratospheric water vapor distribution in winter 2010 compared to that of climatology (Fig. 1a) are partly associated with ENSO variability, as mentioned earlier.

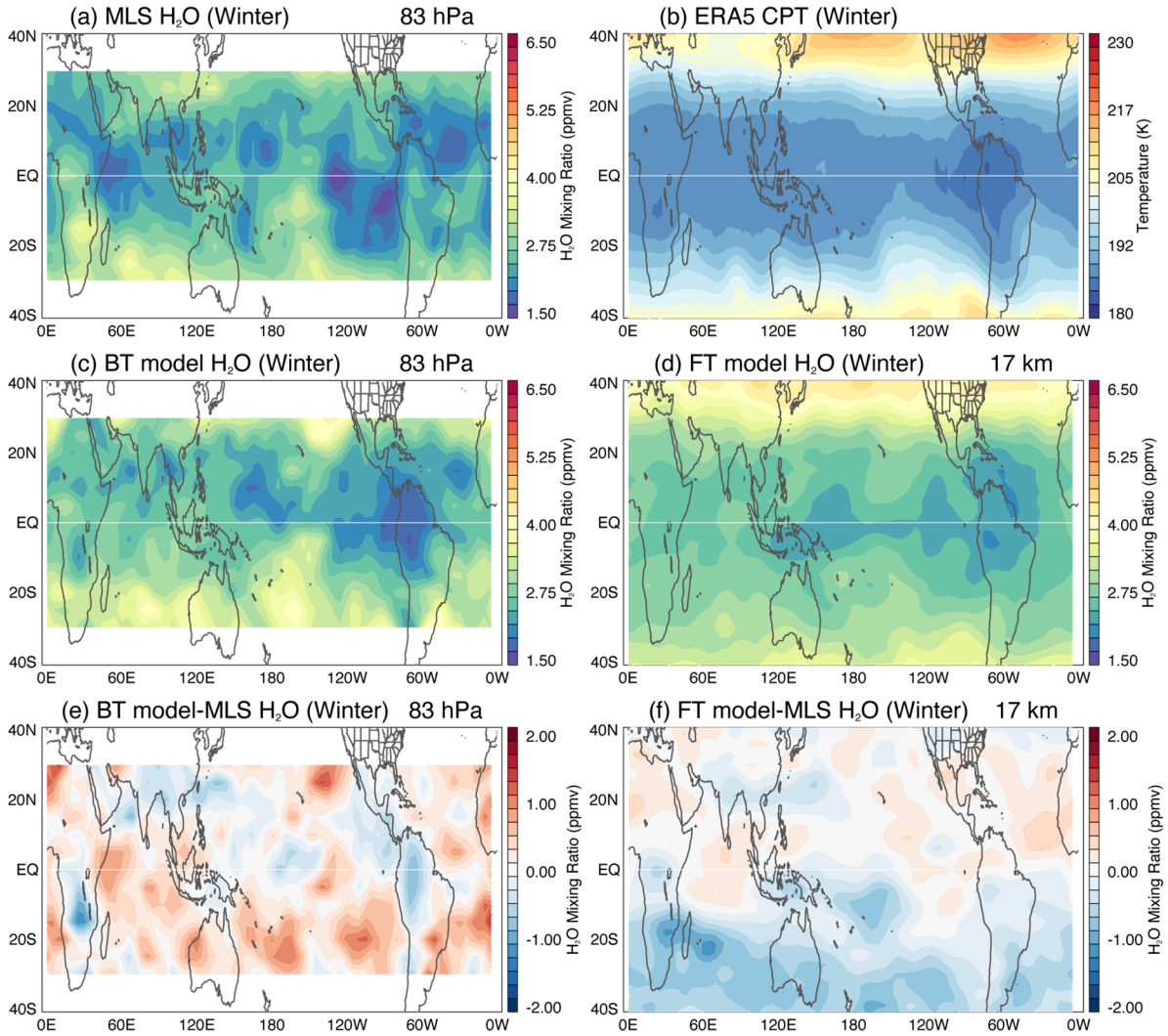


Figure 3: Lower stratospheric (83 hPa) water vapor field in boreal winter (21 February 2010) as observed by MLS (a) and simulated in the backward and forward trajectory models (c and d, respectively) . (e and f) Water vapor difference (model minus MLS) fields. (b) Cold-point tropopause temperature field from ERA5 during the same time period. MLS, ERA5 and FT model data are averaged over seven days centered on 21 February 2010. 1-2-1 smoothing is applied to all the data for presentation purposes.

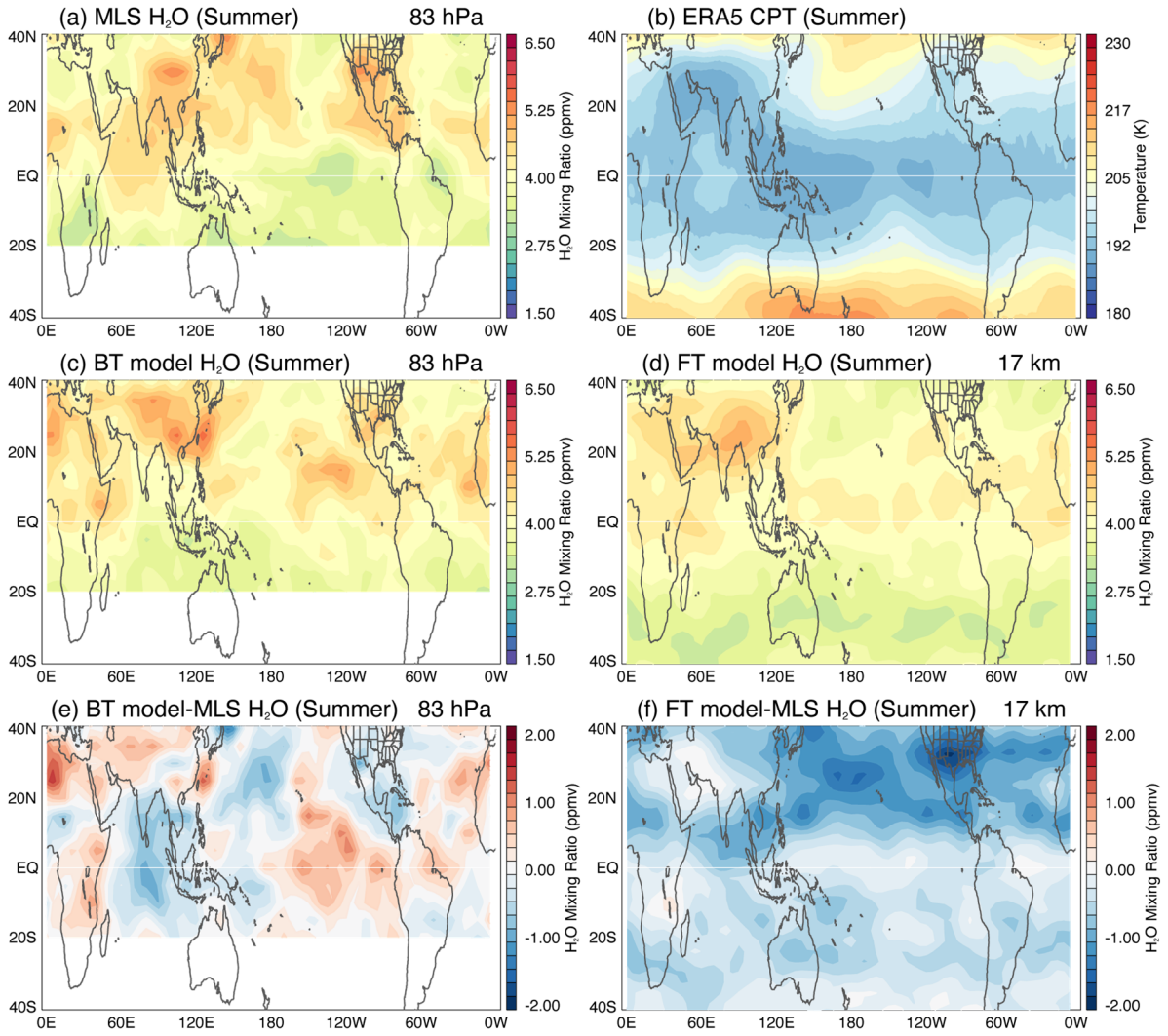


Figure 4: Lower stratospheric (83 hPa) water vapor field in boreal summer (22 August 2010) as observed by MLS (a) and simulated in the backward and forward trajectory models (c and d, respectively) . (e and f) Water vapor difference (model minus MLS) fields. (b) Cold-point tropopause temperature field from ERA5 during the same time period. MLS, ERA5 and FT model data are averaged over seven days centered on 22 August 2010. 1-2-1 smoothing is applied to all the data for presentation purposes.

The lower stratospheric water vapor field during boreal summer 2010 (Fig. 4a) consists of large enhancements over the Asian and North American monsoon regions, as seen in climatology (Fig. 1). The seven-day mean water vapor field centered on 22 August 2010 (i.e., 19-25 August 2010) indicates a relatively moist stratosphere over the western and central Pacific, which may be associated with the transient eastward transport of moist air from the Asian monsoon region. The 83-hPa water vapor field simulated in the BT model (Fig. 4c) is dominated by the elevated water vapor mixing ratios over the Asian monsoon, in agreement with observations although there are some differences in the placement of these anomalies due to the simulation being for a single day. The water vapor enhancement over the North American monsoon region is not as large or spatially coherent as in observations. However, it is an

improvement over the previous simulation using the same model (see Fig. 3 in Ueyama et al., 2018) with ~0.2 ppmv increase in the regional mean water vapor mixing ratio. The main difference between the two versions is the modification of the convective cloud top heights over the northern midlatitudes, as described in Section 2.2.

Lower stratospheric water vapor over the two summer monsoon regions is also enhanced in the FT model (Fig. 4d), but the model is generally too dry compared to MLS observations (Fig. 4f). One possible explanation is that the FT model is underestimating the spread of cirrus anvils that would widen the convective moistening impact. A second explanation is that the height of the convection is underestimated. The sensitivity of global lower stratospheric water vapor to convective cloud tops of varying heights over various regions in the two models will be investigated in a future study. In the current setting, biases are no more than ~10% of the observed domain-averaged water vapor mixing ratios in the BT model for both winter and summer 2010.

Another method for evaluating the models is to compare the simulated cloud fractions to those observed by CALIOP. The BT model simulates the cirrus cloud distributions in the UTLS remarkably well during both seasons with correlation coefficients greater than 0.9, although the model silghtly overestimates the amount of clouds in both seasons (not shown). The FT model also simulates the cirrus cloud distributions reasonably well, but underestimates the cloud fractions by 30% in winter and 48% in summer 2010 compared to CALIOP measurements. The simplified cloud scheme that is coupled to the FT model removes settling particles once they reach the lower edge of the cloud domain, which would tend to underestimate the cloud occurrence. Therefore, we will primarily use the FT model to examine the amplitude of the year-to-year variations in the convective impact relative to its mean, which is expected to be more robust as it represents the relative contribution of convection on lower stratospheric water vapor on long (e.g., longer than synoptic-scale) time scales. Interannual variations in lower stratospheric water vapor are simulated well in the FT model, as will be shown in Section 3.2.

### *3.1.2 Convective impact*

To investigate the impact of convection on lower stratospheric humidity, we have also run a set of simulations without the convective effects. In the "no convection" simulations, trajectory intersections with convection are simply ignored (i.e., no changes are made to the water vapor or ice at that time). The convective impact on lower stratospheric water vapor is then quantified by subtracting the 83-hPa water vapor mixing ratios simulated without convection from those simulated with convection of their respective models.

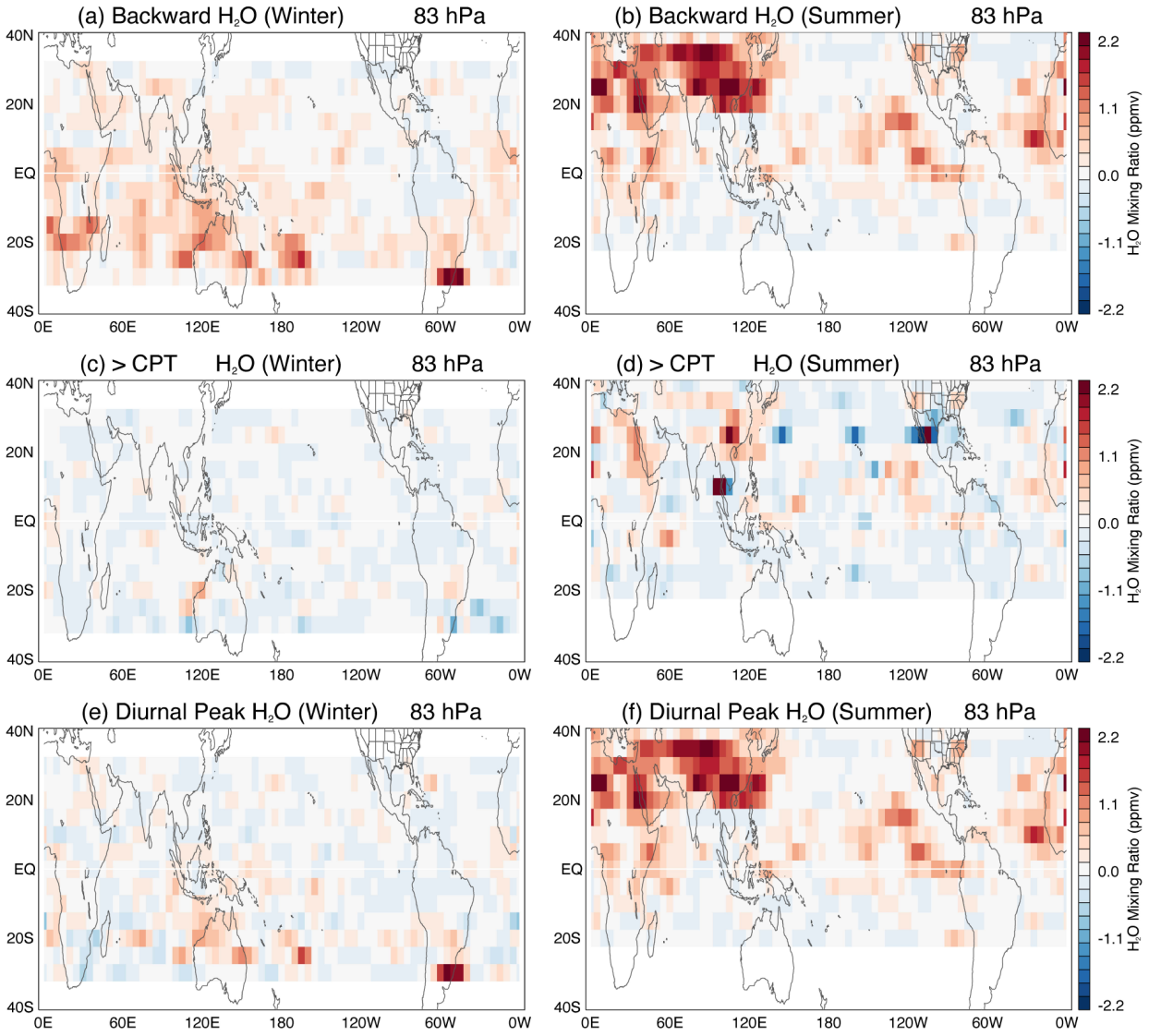


Figure 5: Impact of convection on the lower stratospheric (83 hPa) water vapor field during (left) winter and (right) summer 2010 based on the backward trajectory model approach: impact of (a, b) all convective clouds above 350 K, (c, d) convective cloud tops above the local cold-point tropopause, and (e, f) diurnal peak in convective cloud top height.

The convective impact on lower stratospheric water vapor during winter and summer 2010 estimated from the BT model is shown in Figure 5. It is evident that the overall effect of convection is a moistening of the lower stratosphere (Figs. 5a and b). In winter, convective hydration occurs mostly south of the equator with largest moistening over northern Australia where the relatively frequent deep convection occurs. Convective impact is minmal over the cold temperature region of the western tropical Pacific because convectively-injected water vapor and ice are quickly removed by the freeze-drying process. In summer, convection increases the humidity over the Asian monsoon region by ~1 ppmv (regional mean increase of 30%), dominating the global convective impact. Convective moistening over the North American monsoon region is not as large (0.2 ppmv corresponding to a regional mean increase

of 5%) as that over the Asian monsoon and focused over the eastern tropical Pacific. Northern Africa is also moistened by convection, contributing to the (BT) model moist bias compared to MLS observations (Fig. 3f).

The domain-averaged moistening is about 0.3 ppmv or 10% in both seasons (0.28 ppmv in winter, 0.32 ppmv in summer), in agreement with Schoeberl et al. (2014). Sensitivity simulations with the BT model indicate that convection moistens the lower stratosphere by increasing the relative humidity of the subsaturated environment; the impact of convectively-detrained ice crystals in aging anvils is small, in agreement with Ueyama et al. (2020) for the winter TTL. The convective impact is larger (i.e., approximately 0.4 ppmv in winter and 0.6 ppmv in summer) and more spatially uniform in the FT model (not shown). It is reasonable to expect some differences in the results based on the backward and forward trajectory models due to differences in the modelling approaches (Table 1). First, the two models use different reanalysis fields for calculating the trajectories and for simulating the cloud processes. Ideally, the two models will use the same reanalysis data, but the models are each set up to run with specific reanalysis products. The BT model is configured to use high-resolution ERA5 data over a short time period, while the FT model is configured to use lower resolution MERRA-2 data over multiple years. Tegtmeier et al. (2020) investigated the differences in the TTL temperature and tropopause characteristics from various reanalyses data and found that TTL temperatures from ERA5 are colder (by ~0.5 K) than those of MERRA-2 in the climatological mean as well as in year 2010. This suggests that differences in the temperature data alone would yield a drier lower stratosphere in the BT model using ERA5 temperatures than in the FT model using MERRA-2 temperatures, opposite of our findings. Second, a few of the BTs terminate in stratospheric locations, and thus will be wetter than the FTs that move through the tropopause. Third, as noted earlier, the microphysical scheme of the BT model allows for the sublimation of falling hydrometeors. The overall moistening of the UTLS by this effect in the BT model likely counteracts the differences due to the reanalysis temperatures. Fourth, the different heating rates could impact the model results. Sensitivity simulations using ERA5 heating rates in the BT model suggest that the convective impact on lower stratospheric water vapor varies by only a few percent in winter and summer 2010. Overall, the differences in the two models provide us with some assessment of the uncertainty in the calculation.

To evaluate the importance of extreme deep convection overshooting the local tropopause on global lower stratospheric water vapor budget, we run the BT model with convective cloud tops capped at the cold-point tropopause altitudes derived from ERA5 reanalysis data. We find that convection overshooting the cold-point tropopause increases global lower stratospheric humidity by only 1% in boreal winter and summer 2010 (Figs. 5c and d), which is an order of magnitude smaller than the total convective impact of 10%. Regionally, tropopause-overshooting convection moistens the lower stratosphere over the Asian monsoon region by ~6% during summer. The largest impact during winter is observed over northern Australia and southeastern coast of South America, which correspond to the regions of frequent extreme deep convection. While the overall effect of tropopause-overshooting convection is a small moistening of the lower stratosphere, subsequent dehydration may occur if convectively-influenced parcel encounters supersaturated air downstream of convection; in this case, water vapor in excess of saturation condenses on convectively-detrained ice crystals, and the humidity of the environmental air is brought down to saturation. The small impact of tropopause-overshooting convection on lower stratospheric water vapor is consistent with the infrequent occurrence of these events (approximately 5% and 8% of all convective clouds in winter and

549 summer, respectively) and the findings of Jensen et al. (2020). In general, the globally averaged
550 lower stratospheric water vapor exhibits weak sensitivity to small (on the order of a kilometer)
551 changes in the height of the global convective cloud tops (not shown).

552 Convection exhibits a distinct diurnal cycle with a large peak around 1630 local time over
553 land and a smaller peak at around 0430 local time over the ocean (Liu & Liu, 2016; Liu &
554 Zipser, 2005. We examine the impact of the diurnal peak in convective cloud top altitudes by
555 first constructing time-varying global convective cloud top altitude data without the diurnal peak
556 in convection: the three-hourly convective cloud top altitudes (00, 03, 06, 09, 12, 15, 18, 21Z) on
557 a given day are replaced with the cloud top altitude at 00Z of that same day. We then trace the
558 backward trajectories through this modified convection dataset to examine the sensitivity of
559 lower stratospheric humidity to the diurnal peak in convective cloud top altitudes. We find that
560 the diurnal peak in convection moistens the lower stratosphere by approximately 0.1 ppmv in
561 winter and 0.3 ppmv in summer (Figs. 5e and c). In other words, the diurnal peak in convection
562 is responsible for about half of the total convective moistening of the lower stratosphere during
563 winter and nearly all of the convective moistening during summer. The impact of the diurnal
564 variability of convective cloud tops over various regions will be explored in detail in a future
565 study.

566

567 **3.2 Interannual variability**

568 In this section, we use the FT model to examine the year-to-year variability in lower
569 stratospheric water vapor as well as the variations in the convective impact. The time series of
570 domain-averaged water vapor mixing ratios at the 83 hPa level in winter and summer of each
571 year from 2006 to 2016 are shown in Figure 6. The model captures the year-to-year variability
572 in lower stratospheric water vapor remarkably well, as seen by the good agreement with MLS
573 observations. During this time period, the global lower stratospheric water vapor varied between
574 ~2.8 to ~4 ppmv in winter and between ~3.5 to ~4.3 ppmv in summer. Winter 2010 appeared to
575 have been an average year, whereas summer 2010 appeared to have been a relatively moist year
576 during this time period.

577 Also shown are domain-averaged water vapor mixing ratios in the simulation without
578 convection (blue lines). As expected, the lower stratosphere in the simulation without
579 convection is much drier than that of the simulation with convection. However, even without the
580 impacts of convection, lower stratospheric water vapor varies in a similar manner as the
581 observations with coincident peaks and valleys. This suggests that the interannual variability in
582 global lower stratospheric water vapor is largely controlled by processes other than convection,
583 namely by TTL temperatures as found by many previous studies (Fueglistaler et al., 2009;
584 Randel et al., 2004; Randel & Park, 2019). Based on the linear correlations between the
585 observed and simulated water vapor time series, we estimate that convection explains
586 approximately 10% (30%) of the total variance in MLS water vapor during winter (summer) over
587 this time period.

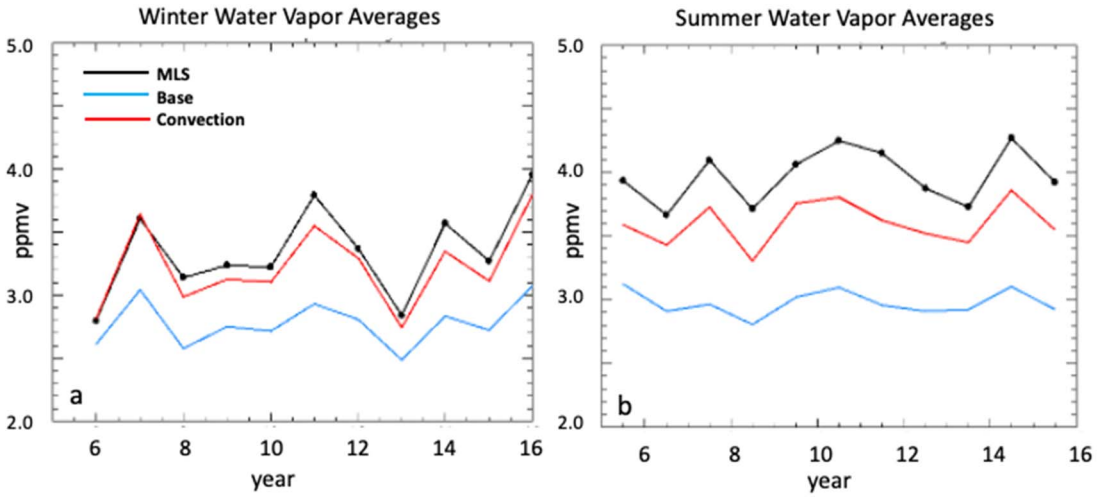


Figure 6: Time series of the domain averaged (30°S-30°N for winter, 20°S-50°N for summer) lower stratospheric water vapor mixing ratio during (a) winter and (b) summer 2006-2016: MLS observations (black), model without convection (blue), and model with convection (red). Winter is the average of December through February of the year of January, and June through August is represented as the summer value.

The year-to-year variations in the convective impact on the global lower stratospheric water vapor budget is quantified by calculating the water vapor difference fields (i.e., simulation with convection minus simulation without convection) for each season and year. The domain-averaged differences are plotted in a time series for winter and summer separately in Figure 7. When compared to the time series of lower stratospheric water vapor (Fig. 6), we find that winters/summers with relatively large convective impact generally correspond to winters/summers with relatively moist stratosphere (e.g., winters 2007, 2011 2014 and 2016; summers 2007, 2010 and 2014) and vice versa. The relationship is less clear during winter compared to summer. Overall, the FT model simulations suggest that convection increases water vapor by approximately 0.45 ppmv in winter and 0.62 ppmv in summer, with a standard deviation of 0.15 and 0.10 ppmv, respectively. The amplitudes of the interannual variations in the convective impact in boreal winter and summer are therefore approximately 35% and 17% of their respective means. Combining these results with those based on the BT model (i.e., domain-averaged moistening is about 0.3 ppmv), we estimate the impact of convection on the global lower stratospheric water budget to be approximately 0.3 with year-to-year variations of 0.05 to 0.1 ppmv during 2006-16.

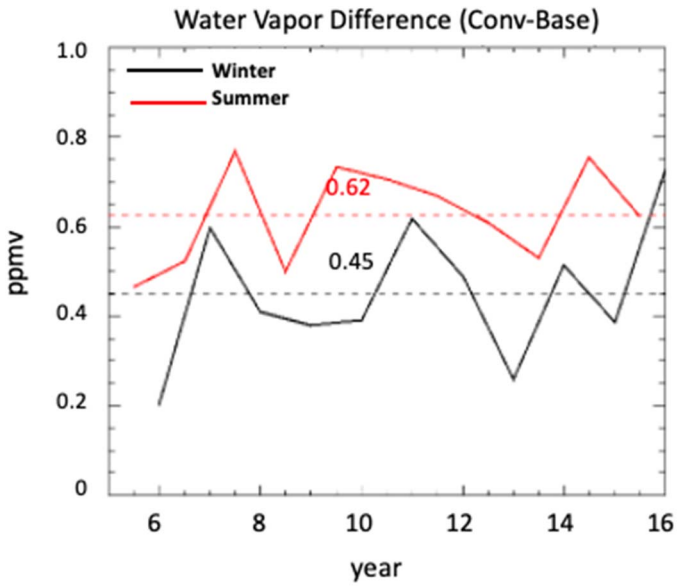


Figure 7: Year-to-year variability of the domain-averaged (30°S-30°N for winter, 20°S-50°N for summer) convective impact on the lower stratospheric water vapor mixing ratio during winters (black) and summers (red) 2006-16. The long-term mean convective impact in the two seasons is shown (in ppmv). Winter is the average of December through February of the year of January, and June through August is represented as the summer value.

## 4 Discussion

The results of this study clearly show that convection in the upper troposphere hydrates the lower stratosphere. Our results further demonstrate the limited role of extreme deep convection overshooting the tropopause on the global lower stratospheric water vapor budget. Given the infrequent occurrence of convective clouds that extend above the tropopause, the primary mechanism of convective moistening of the lower stratosphere must be through the detrainment of saturated air and ice into the tropical uppermost troposphere. How can moistening of the upper troposphere affect stratospheric water vapor when observations suggest that stratospheric water vapor mixing ratio is primarily controlled by the cold-point tropopause temperature (e.g., Randel & Park, 2019)?

Aircraft observations in the TTL (e.g., Jensen et al., 2017) indicate that a significant fraction of air near the tropopause is subsaturated. The water vapor mixing ratio of the subsaturated air parcel near the tropopause is primarily determined by moistening and drying events that occur *below* the tropopause. Convection shifts the relative humidity distribution of subsaturated air parcels in the upper troposphere toward higher relative humidity values, and thus increases the water vapor in the stratosphere.

As evidence of this process, Figure 8 shows the relative humidity distribution of FT air parcels in the upper TTL (100 hPa; between 60°-180°E and 25°S - 25°N) during winter and summer 2010. In both seasons, the relative humidity distribution shifts to higher values for the simulation with convection. The distribution is quite similar to that observed during NASA Airborne Tropical Tropopause Experiment (ATTREX; Jensen et al., 2017) except that the peak at 100% relative humidity is broader and higher in the observations compared to the model.

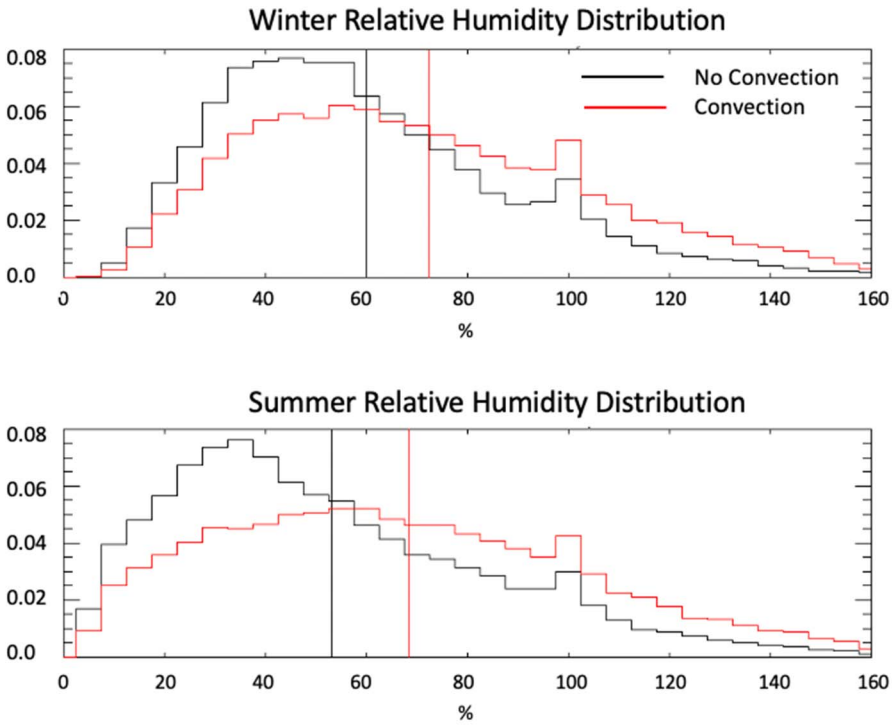


Figure 8: Relative humidity distributions of parcels in the forward trajectory model simulations for (top) winter and (bottom) summer 2010: model without convection (black), and model with convection (red). The relative humidity distribution is calculated for parcels at the 100 hPa level between 60°E and 180°E, and 25°S to 25°N. Vertical lines indicate the mean of each distribution.

## 5 Summary and Conclusions

Two complementary modeling approaches are used to investigate the impact of convection on the global lower stratospheric water vapor budget. The backward trajectory method provides direct estimates of the water vapor in the global lower stratosphere at a given valid time. The forward trajectory method provides a time series of the full three-dimensional water vapor field throughout the stratosphere from a single simulation permitting calculations of the interannual variability of stratospheric water vapor. One of the important differences between the backward and forward trajectory model approaches is that the backward trajectory model is coupled to a detailed cloud microphysical scheme that properly treats the vertical redistribution of water vapor by ice crystals. We therefore use the backward trajectory model to estimate the magnitude of the convective impact during boreal winter and summer 2010, and use the FT model to examine the relative amplitude of the year-to-year variations in the convective impact. Despite their different approaches, both models simulate the lower stratospheric water vapor field in boreal winter and summer 2010 reasonably well.

The backward trajectory model indicates that convection moistens the lower stratosphere by about 0.3 ppmv (0.28 ppmv in winter, 0.32 ppmv in summer), which accounts for approximately 10% of the global lower stratospheric humidity (11% in winter, 9% in summer), in agreement with past studies (e.g., Schoeberl et al., 2014; Ueyama et al., 2014, 2015). Convection has a larger (~1 ppmv or regional mean increase of 30%) impact on the humidity of

667 the lower stratosphere at the 83 hPa level over the Asian summer monsoon region. In both
668 seasons, most of the convective moistening is associated with the rapid saturation of the
669 convectively-influenced atmospheric column rather than by the sublimation of convectively-
670 detrained ice crystals in aging anvils. Global lower stratospheric humidity exhibits weak
671 sensitivity to small changes in the height of the global convective cloud tops, including to
672 extreme deep convection overshooting the cold-point tropopause which increases global lower
673 stratospheric humidity by only 1% in both seasons. The diurnal peak in convection accounts for
674 about half of the total convective moistening of the lower stratosphere during winter and nearly
675 all of the convective moistening during summer.

676 Simulations with the forward trajectory model show that the interannual variability in
677 global lower stratospheric water vapor during 2006-16 is largely controlled by processes other
678 than convection (i.e., TTL temperatures). Convection contributes between 0.05 and 0.1 ppmv of
679 the year-to-year variability in stratospheric water vapor. Years with with relatively large
680 convective impact generally correspond to years with relatively moist stratosphere, and vice
681 versa. Combining the forward trajectory model results with those based on the backward
682 trajectory model, we estimate the impact of convection on the global lower stratospheric water
683 vapor budget to be a moistening of approximately 0.3 with year-to-year variations of up to 0.1
684 ppmv during 2006-16.

685 Analyses of parcel relative humidities in the forward trajectory model show that
686 convection in the upper troposphere shifts the relative humidity distribution of upper
687 tropospheric parcels towards higher humidities. Some of these parcels in the upper troposphere
688 with high relative humidities do not undergo ice nucleation during their ascent, and ultimately
689 increase the globally averaged stratospheric water vapor. In other words, the dominant
690 mechanism of convective hydration of the lower stratosphere is via the detrainment of saturated
691 air and ice into the tropical uppermost troposphere, followed by ascent into the stratosphere.
692 Extreme deep convection overshooting the tropopause, which is rare relative to convection
693 reaching the upper troposphere, has minimal impact on the global lower stratospheric water
694 vapor budget.

695 In summary, the impact of convection on the global lower stratospheric water vapor
696 budget is realtively small in the current climate, although it can be much larger on a regional
697 basis such as over the summer monsoon regions. Our results suggest that a convective impact on
698 the global lower stratospheric humidity of more than 10% would require significant changes in
699 global convective activity from the current climate. Nonetheless, as the summer monsoon
700 anticyclone and convection have been shown to substantially influence the distribution of trace
701 gases in the UTLS (Dethof et al., 1999; Garny & Randel, 2016; Gettelman et al., 2004; Jensen et
702 al., 2020; Orbe et al., 2015; Pan et al., 2016; Randel & Park, 2006; Randel et al., 2012; Santee et
703 al., 2017; Schwartz et al., 2013; Smith et al., 2017), a significant change in monsoon convection
704 and/or cirrus cloud distribution in future climate could potentially have a measureable effect on
705 the composition of the stratosphere.

706

707 **Acknowledgments**

708 All data used in this study are publicly available at no charge, including the satellite-derived
709 convective cloud top dataset available at https://bocachica.arc.nasa.gov/nasaarc_cldalt/. This
710 work is supported by NASA grants in the Upper Atmospheric Composition Observations and

Aura Science Team (Grant 80NSSC20K1235) programs as well as with funding from the Earth Venture Suborbital (EVS-3) Dynamics and Chemistry of the Summer Stratosphere (DCOTSS) project. RU is also supported by the Atmospheric Composition Program through the NASA Internal Scientist Funding Model. The National Center for Atmospheric Research is operated by the University Corporation for Atmospheric Research, under sponsorship of the National Science Foundation. Any opinions, finding, and conclusions or recommendations expressed in this publication are those of the author(s) and do not necessarily reflect the views of the National Science Foundation.

## References

Adler, R. F.. & Mack, R. A. (1986), Thunderstorm cloud top dynamics as inferred from satellite observations and a cloud top parcel model. *Journal of the Atmospheric Sciences*, *43 (18)*, 1945-1960. https://doi.org/10.1175/1520-0469(1986)043<1945:TCTDAI>2.0.CO;2

Anderson, J. G., Wilmouth, D. M., Smith, J. B., & Sayres, D. S. (2012), UV dosage levels in summer: Increased risk of ozone loss from convectively injected water vapor. *Science*, *337*, 835-839. https://doi.org/10.1126/science.1222978

Avery, M., A., Davis, S. M., Rosenlof, K. H., Ye, H., & Dessler, A. E. (2017), Large anomalies in lower stratospheric water vapour and ice during the 2015-2016 El Niño. *Nature Geoscience*, *10*, 405-409. https://doi.org/10.1036/ngeo2961

Banerjee, A., Chiodo, G., Previdi, M., Ponater, M., Conley, A. J., & Polvani, L. M. (2019), Stratospheric water vapor: an important climate feedback. *Climate Dynamics*, *53*, 1697-1710. https://doi.org/10.1007/s00382-019-04721-4

Bergman, J. W., Jensen, E. J., Pfister, L., & Yang, Q. (2012), Seasonal differences of vertical-transport efficiency in the tropical tropopause layer: On the interplay between tropical deep convection, large-scale vertical ascent, and horizontal circulations. *Jounral of Geophysical Research: Atmospheres*, *117*(D5). https://doi.org/10.1029/2011JD016992

Boehm, M. T., & Verlinde, J. (2000), Stratospheric influence on upper tropospheric tropical cirrus. *Geophysical Research Letters*, *27(19)*, 3209-3212. https://doi.org/10.1029/2000GL011678

Brewer, A. W. (1949), Evidence for a world circulation provided by the measurements of helium and water vapor distribution in the stratosphere. *Quarterly Journal of the Royal Meteorological Society*, *75*, 351-363. https://doi.org/10.1002/qj.49707532603

Chae, J. H., Wu, D. L., Read, W. G., & Sherwood, S. C. (2011), The role of tropical deep convective clouds on temperature, water vapor, and dehydration in the tropical tropopause layer (TTL). *Atmospheric Chemistry and Physics*, *11*, 3811-3821. https://doi.org/10.5194/acp-11-3811-2011

Chang, K.-W., & L'Ecuyer, T. (2020), Influence of gravity wave temperature anomalies and their vertical gradients on cirrus clouds in the tropical tropopause layer – a satellite-based view. *Atmospheric Chemistry and Physics*, *20*, 12499-12514. https://doi.org/10.5194/acp-20-12499-2020

751 Chou, C., & Chen, C.-A. (2010), Depth of convection and the weakening of tropical circulation
752 in global warming. *Journal of Climate*, *23*, 3019-3030. https://doi.org/10.1175/2010JCLI3383.1

753 Corti, T., Luo, B. P., de Reus, M., Brunner, D., Cairo, F., Mahoney, M. J., et al. (2008),
754 Unprecedented evidence for deep convection hydrating the tropical stratosphere. *Geophysical*
755 *Research Letters*, *35*(10). https://doi.org/10.1029/2008GL033641

756 Danielsen, E. F. (1982), A dehydration mechanism for the stratosphere. *Geophysical Research*
757 *Letters*, *9*(6), 605-608. https://doi.org/10.1029/GL009i006p00605

758 Danielsen, E. F. (1983), In situ evidence of rapid, vertical, irreversible transport of lower
759 tropospheric air into the lower tropical stratosphere by convective cloud turrets and by larger-
760 scale upwelling in tropical cyclones. *Jounral of Geophysical Research: Atmospheres*, *98*(D5),
761 8665-8681. https://doi.org/10.1029/92JD02954

762 Dessler, A. E., Schoeberl, M. R., Wang, T., Davis, S. M., & Rosenlof, K. H. (2013),
763 Stratospheric water vapor feedback. *Proceedings of the National Academy of Sciences*, *110 (45)*,
764 18087-18091. https://doi.org/10.1073/pnas.1310344110

765 Dessler, A. E., Ye, H., Wang, T., Schoeberl, M. R., Oman, L. D., Douglass, A. R., et al. (2016),
766 Transport of ice into the stratosphere and the humidification of the stratosphere over the 21st
767 century. *Geophysical Research Letters*, *43*(5), 2323-2329.
768 https://doi.org/10.1002/2016GL067991

769 Dethof, A., O'Neill, A., Slingo, J. M., & Smit, H. G. J. (1999), A mechanism for moistening the
770 lower stratosphere involving the Asian summer monsoon. *Quarterly Journal of the Royal*
771 *Meteorological Society*, *125*(556), 1079-1106. https://doi.org/10.1002/qj.1999.49712555602

772 Dinh, T., Podglajen, A., Hertzog, A., Legras, B., & Plougonven, R. (2016), Effect of gravity
773 wave temperature fluctuations on homogeneous ice nucleation in the tropical tropopause layer.
774 *Atmospheric Chemistry and Physics*, *16*, 35-46. https://doi.org/10.5194/acp-16-35-2016

775 Dvortsov, V. L., & Solomon, S. (2001), Response of the stratospheric temperatures and ozone to
776 past and future increase in stratospheric humidity. *Jounral of Geophysical Research:*
777 *Atmospheres*, *106*(D7), 7505-7514. https://doi.org/10.1029/2000JD900637

778 Forster, P. M. de F., & Shine, K. P. (1999), Stratospheric water vapor changes as a possible
779 contributor to observed stratospheric cooling. *Geophysical Research Letters*, *26*, 3309-3312.
780 https://doi.org/10.1029/1999GL010487

781 Forster, P. M. de F., & Shine, K. P. (2002), Assessing the climate impact of trends in
782 stratospheric water vapor. *Geophysical Research Letters*, *29*(6), 10-1-10-4.
783 https://doi.org/10.1029/2001GL013909

784 Frey, W., Borrmann, S., Fierli, F., Weigel, R., Miev, V., Matthey, R., et al. (2014), Tropical deep
785 convective life cycle: Cb-anvil cloud microphysics from high-altitude aircraft observations.
786 *Atmospheric Chemistry and Physics*, *14*, 13223-13240. https://doi.org/10.5194/acp-14-13223-
787 2014

788 Fueglistaler, S., Bonazzola, M., Haynes, P. H., & Peter, T. (2005), Stratospheric water vapor
789 predicted from the Lagrangian temperature history of air entering the stratosphere in the tropics.
790 *Journal of Geophysical Research, 110*, D08107. https://doi.org/10.1029/2004JD005516

Fueglistaler, S., & Baker, M. B. (2006), A modelling study of the impact of cirrus clouds on the moisture budget of the upper troposphere. *Atmospheric Chemistry and Physics*, *6*, 1425-1434. https://doi.org/10.5194/acp-6-1425-2006

Fueglistaler, S., Dessler, A. E., Dunkerton, T. J., Folkins, I., Fu, Q., & Mote, P. W. (2009), Tropical tropopause layer. *Reviews of Geopohysics*, *47*, RG1004. https://doi.org/10.1029/2008RG00267

Fujiwara, M., Iwasaki, S., Shimizu, A., Inai, Y., Shiotani, M., Hasebe, F., et al. (2009), Cirrus observations in the tropical tropopause layer over the western Pacific. *Journal of Geophysical Research: Atmospheres, 114*(D9). https://doi.org/10.1029/2008JD011040

Garrett, T. J., Heymsfield, A. J., McGill, M. J., Ridley, B. A., Baumgardner, D. G., Bui, T. P., et al. (2004), Convective generation of cirrus near the tropopause. *Journal of Geophysical Research: Atmospheres, 109*(D21). https://doi.org/10.1029/2004JD004952

Garrett, T. J., Dean-Day, J., Liu, C., Barnett, B., Mace, G., Baumgardner, D., et al. (2006), Convective formation of pileus cloud near the tropopause. *Atmospheric Chemistry and Physics*, *6*, 1185-1200. https://doi.org/10.5194/acp-6-1185-2006

Gasparini, B., Blossey, P. N., Hartmann, D. L., Lin, G., & Fan, J. (2019), What drives the life cycle of tropical anvil clouds? *Journal of Advances in Modeling Earth Systems*, *11*(8), https://doi.org/10.1029/2019MS001736

Gelaro, R., McCarty, W., Suárez, M. J., Todling, R., Molod, A., Takacs, L., et al. (2017), The Modern-Era Retrospective Analysis for Research and Applications, Version 2 (MERRA-2). *Journal of Climate*, *30*(14), 5419-5454. https://doi.org/10.1175/JCLI-D-16-0758.1

Gettelman, A., Salby, M. L., & Sassi, F. (2002), Distribution and influence of convection in the tropical tropopause region. *Journal of Geophysical Research: Atmospheres, 107*(D10). https://doi.org/10.1029/2001JD001048

Gettelman, A., Kinnison, D. E., Dunkerton, T. J., & Brasseur, G. P. (2004), Impact of monsoon circulations on the upper troposphere and lower stratosphere. *Journal of Geophysical Research: Atmospheres, 109*(D22). https://doi.org/10.1029/2004JD004878

Kärcher, B., Hendricks, J., & Lohmann, U. (2006), Physically based parameterization of cirrus cloud formation for use in global atmospheric models. *Journal of Geophysical Research: Atmospheres, 111*(D1). https://doi.org/10.1029/2005JD006219

Hao, A. Y., Kakar, R. K., Neeck, S., Azarbarzin, A. A., Kummerow, C. D., Kojima, M., et al. (2014), The Global Precipitation Measurement Mission. *Bulletin of the American Meteorological Society*, *95*, 701-722. https://doi.org/10.1175/BAMS-D-13-00164.1.

Hartmann, D. L., Holton, J. R., & Fu, Q. (2001), The heat balance of the tropica tropopause, cirrus, and stratospheric dehydration. *Geophysical Research Letters*, *28*(10), 1969-1972. https://doi.org/10.1029/2000GL012833

Hatsushika, H., & Yamazaki, K. (2003), Stratosheric drain over Indonesia and dehydration within the tropical tropopause layer diagnosed by air parcel trajectories. *Journal of Geophysical Research: Atmospheres, 108*(D19). https://doi.org/10.1029/2002JD002986

Held, I. M., & Soden, B. J. (2006), Robus responses of the hydrological cycle to global warming. *Journal of Climate*, *19*(21), 5686-5699. https://doi.org/10.1175/JCLI3990.1

Henderson, D. S., L'Ecuyer, T., Stephens, G., Partain, P., & Sekiguchi, M. (2013), A multisensory perspective on the radiative impacts of clouds and aerosols. *Journal of Applied Meteorology and Climatology, 52*, 853-871. https://doi.org/10.1175/JAMC-D-12-025.1

Hersbach, H., Bell, B., Berrisford, P., Hirahara, S., Horányi, A., Muñoz-Sabater, J., et al. (2020), The ERA5 global reanalysis. *Quarterly Journal of the Royal Meteorological Society*, *146*(730), 1999-2049. https://doi.org/10.1002/qj.3803

Holton, J. R., Haynes, P. H., McIntyre, M. E., Douglass, A. R., Rood, R. B., & Pfister, L. (1995), Stratosphere-troposphere exchange. *Reviews of Geopohysics*, *33*(4), 403-439. https://doi.org/10.1029/95RG02097

Holton, J. R., & Gettelman, A. (2001), Horizontal transport and the dehydration of the stratosphere. *Geophysical Research Letters*, *28*(14), 2799-2802. https://doi.org/10.1029/2001GL013148

Huang, Y., Wang, Y., & Huang, H. (2020), Stratospheric water vapor feedback disclosed by a locking experiment. *Geophysical Research Letters*, *47*(12), e2020GL087987. https://doi.org/10.1029/2020GL087987

Hurst, D. F., Read, W. G., Vömel, H., Selkirk, H. B., Rosenlof, K. H., Davis, S. M., et al. (2016), Recent divergences in stratospheric water vapor measurements by frost point hygrometers and the Aura Microwave Limb Sounder. *Atmospheric Measurement Techniques*, *9*, 4447-4457. https://doi.org/10.5194/amt-9-4447-2016

Immler, F., Krüger, K., Fujiwara, M., Verver, G., Rex, M., & Schrems, O. (2008), Correlation between equatorial Kelvin waves and the occurrence of extremely thin ice clouds at the tropical tropopause. *Atmospheric Chemistry and Physics*, *8*, 4019-4026. https://doi.org/10.5194/acp-8-4019-2008

Jensen, E. J., & Pfister, L. (2004), Transport and freeze-drying in the tropical tropopause layer. *Journal of Geophysical Research, 109*, D02207. https://doi.org/doi:10.1029/2003JD004022

Jensen, E. J., Pfister, L., & Toon, O. B. (2011), Impact of radiative heating, wind shear, temperature variability, and microphysical processes on the structure and evolution of thin cirrus in the tropical tropopause layer. *Journal of Geophysical Research, 116*(D12209). https://doi.org/10.1029/2010JD015417

Jensen, E. J., Pfister, L., Jordan, D. E., Bui., T. V., Ueyama, R., Singh, H. B., et al. (2017), The NASA Airborne Tropical Tropopause Experiment: High-Altitude Aircraft Measurements in the Tropical Western Pacific. *Bulletin of the American Meteorological Society*, *98*(1), 129-143. https://doi.org/10.1175/BAMS-D-14-00263.1

Jensen, E. J., Thornberry, T. D., Rollins, A. W., Ueyama, R., Pfister, L., Bui, T., et al. (2017), Physical processes controlling the spatial distributions of relative humidity in the tropical tropopause layer over the Pacific. *Journal of Geophysical Research: Atmospheres, 122*, 6094-6107. https://doi.org/10.1029/2017JD026632

Jensen, E. J., Pan, L. L., Honomichl, S., Diskin, G. S., Krämer, & M., Spelten, N., et al. (2020), Assessment of observational evidence for direct convective hydration of the lower stratosphere. *Journal of Geophysical Research: Atmospheres, 125*, e2020JD032793. https://doi.org/10.1029/2020JD032793

Kelly, K. K., Proffitt, M. H., Chan, K. R., Loewenstein, M., Podolske, J. R., Strahan, S. E., et al. (1983), Water vapor and cloud water measurements over Darwin during the STEP 1987 tropical mission. *Journal of Geophysical Research, 98*(D5), 8713-8723 https://doi.org/10.1029/92JD02526

Kiehl, J. T., & Solomon, S. (1986), On the radiative balance of the stratosphere. *Journal of the Atmospheric Sciences*, *43*(14). https://doi.org/10.1175/1520-0469(1986)043<1525:OTRBOT>2.0.CO;2

Kim, J.-E., Alexander, M. J., Bui, T. P., Dean-Day, J. M., Lawson, R. P., Woods, S., et al. (2016), Ubiquitous influence of waves on tropical high cirrus clouds. *Geophysical Research Letters*, *43*, 5895-5901. https://doi.org/10.1029/2016GL069293

Kim, J., Randel, W. J., & Birner, T. (2018), Convectively driven tropopause-level cooling and its influences on stratospheric moisture. *Journal of Geophysical Research: Atmospheres, 123*. https://doi.org/10.1029/2017JD027080

Koop, T., Luo B., Tsias, A., & Peter, T. (2000), Water activitiy as the determinant for homogeneous ice nucleation in aqueous solutions. *Nature*, *406*, 611-614. https://doi.org/10.1038/35020537

Krämer, M., Rolf, C., Spelten, N., Afchine, A., Fahey, D., Jensen, E., et al. (2020), A microphysics guide to cirrus – Part 2: Climatologies of clouds and humidity from observations. *Atmospheric Chemistry and Physics*, *20*, 12569-12608. https://doi.org/10.5194/acp-20-12569-2020

Lambert, A., Read, W., & Livesey, N. (2015), *MLS/Aura level2 water vapor (H2O) mixing ratio V004*. Greenbelt, MD: Goddard Earth Sciences Data and Information Services Center (GES DISC)

Lambert, A., Read, W., & Livesey, N. (2020), *MLS/Aura level2 water vapor (H2O) mixing ratio V005*. Greenbelt, MD: Goddard Earth Sciences Data and Information Services Center (GES DISC)

L'Ecuyer, T. S., Wood, N. B., Haladay, T., Stephens, G. L., & Stackhouse Jr., P. W. (2008), Impact of clouds on atmospheric heating based on the R04 CloudSat fluxes and heating rates data set. *Journal of Geophysical Research, 113*, D00A15. https://doi.org/10.1029/2008JD009951

Li, F. & P. Newman (2020), Stratospheric water vapor feedback and its climate impacts in the coupled atmosphere-ocean Goddard Earth Observing System Chemistry-Climate Model. *Climate Dynamics*, *55*, 1585-1595. https://doi.org/10.1007/s00382-020-05348-6

Livesey, N., J., Read., W. G., Wagner, P. A., Froidevaux, L., Santee, M. L., Schwartz, M. J., et al. (2020), *Version 5.0x Level 2 and 3 data quality and description document (Tech. Rep. No. JPL D-105336 Rev. B)*. Jet Propulsion Laboratory, Retrieved from https://mls.jpl.nasa.gov/data/v5-0_data_quality_document.pdf

Livesey, N. J., Read, W. G., Froidevaux, L., Lambert, A., Santee, M. L., Schwartz, M. J., et al. (2021), Investigation and amelioration of long-term instrumental drifts in water vapor and nitrous oxide measurements from the Aura Microwave Limb Sounder (MLS) and their implications for studies of variability and trends. *Atmosospheric Chemistry and Physics, 21,* 15409–15430. https://doi.org/10.5194/acp-21-15409-2021

914 Liu, N. & Liu, C. (2016), Global distribution of deep convection reaching tropopause in 1 year
915 GPM observations. *Journal of Geophysical Research: Atmospheres, 121*(8), 3824-3842.
916 https://doi.org/10.1002/2015JD024430

917 Liu, C. & Zipser, E. J. (2005), Global distribution of convection penetrating the tropical
918 tropopause. *Journal of Geophysical Research: Atmospheres, 110*(D23).
919 https://doi.org/10.1029/2005JD006063

920 Maycock, A. C., Joshi, M. M., Shine, K. P., & Scaife, A. A. (2013), The circulation response to
921 idealized changes in stratospheric water vapor. *Journal of Climate*, *26 (2)*, 454-561.
922 https://doi.org/10.1175/JCLI-D-12-00155.1

923 Mote, P. W., Rosenlof, K. H., McIntyre, M. E., Carr, E. S., Gille J. C., Holton, J. R., et al.
924 (1996), An atmospheric tape-recorder: The imprint of tropical tropopause temperatures on
925 stratospheric water vapor. *Journal of Geophysical Research, 101*, 3989-4006.
926 https://doi.org/10.1029/95JD03422

927 Nielsen, J. K., Larsen, N., Cairo, F., Di Donfrancesco, G., Rosen, J. M., Durry, G., et al. (2007),
928 Solid particles in the tropical lowest stratosphere. *Atmospheric Chemistry and Physics*, *7*, 685-
929 695. https://doi.org/10.5194/acp-7-685-2007

930 Orbe, C., Waugh, D. W., & Newman, P. A. (2015), Air-mass origin in the tropical lower
931 stratosphere: The influence of Asian boundary layer air. *Geophysical Research Letters*, *42*(10),
932 4240-4248. https://doi.org/10.1002/2015GL063937

933 Pan, L. L., Honomichl, S. B., Kinnison, D. E., Abalos, M., Randel, W. J., Bergman, J. W., et al.
934 (2016), Transport of chemical tracers from the boundary laer to stratosphere associated with the
935 dynamics of the Asian summer monsoon. *Jounral of Geophysical Research: Atmospheres*,
936 *121*(23), 14,159-14,174. https://doi.org/10.1029/2016JD025616

937 Pfister, L., Chan, K. R., Bui, T. P., Bowen, S., Legg, M., Gary, B., et al. (1983), Gravity waves
938 generated by a tropical cyclone during the STEP tropical field program: A case study. *Journal of*
939 *Geophysical Research, 98*(D5), 8611-8638 https://doi.org/10.1029/92JD01679

940 Pfister, L., Selkirk, H. B., Jensen, E. J., Schoberl, M. R., Toon, O. B., Browell, E. G., et al.
941 (2001), Aircraft observations of thin cirrus clouds near the tropical tropopause. *Journal of*
942 *Geophysical Research, 106*(D9), 9765-40069786 https://doi.org/10.1029/2000JD900648

943 Potter, B. E., & Holton, J. R. (1995), The role of monsoon convection in the dehydration of the
944 lower tropical stratosphere. *Journal of the Atmospheric Sciences*, *52*(8), 1034-1050.
945 https://doi.org/10.1175/1520-0469(1995)052<1034:TROMCI>2.0.CO;2

946 Poshyvailo, L., Müller, R., Konopka, P., Günther, G., Riese, M., Podglajen, A., et al. (2018),
947 Sensitivities of modelled water vapour in the lower stratosphere: temperature uncertainty, effects
948 of horizontal transport and small-scale mixing. *Atmosospheric Chemistry and Physics, 18,* 8505–
949 8527. https://doi.org/10.5194/acp-18-8508-2018

950 Randel, W. J., Moyer, E., Park, M., Jensen, E. J., Bernath, P. Walker, K., et al. (2012), Global
951 variations of HDO and HDO/$H_2O$ ratios in the upper troposphere and lower stratosphere derived
952 from ACE-FTS satellite measurements. *Jounral of Geophysical Research: Atmospheres*,
953 *117*(D6). https://doi.org/10.1029/2011JD016632

954 Randel, W. J., & Jensen, E. J. (2013), Physical processes in the tropical tropopause layer and
955 their roles in a changing climate. *Nature Geoscience*, *6*, 169-176.
956 https://doi.org/10.1038/ngeo1733

957 Randel, W. J., & Wu, F. (2015), Variability of Zonal Mean Tropical Temperatures Derived from
958 a Decade of GPS Radio Occultation Data, *Journal of the Atmospheric Sciences*, *72*(3), 1261-
959 1275. https://doi.org/10.1175/JAS-D-14-0216.1

960 Randel, W., & Park, M. (2019), Diagnosing observed stratospheric water vapor relationships to
961 the cold point tropical tropopause. *Journal of Geophysical Research: Atmospheres*, *124*.
962 https://doi.org/10.1029/ 2019JD030648

963 Reinares Martinez, I., Evan, S., Wienhold, G., Brioude, J., Jensen, E. J., Thornberry, T. D., et al.
964 (2021), Unprecedented observations of a nascent in situ cirrus in the tropical tropopause layer.
965 *Geophysical Research Letters*, *48*(4), e2020GL090936. https://doi.org/10.1029/2020GL090936

966 Robinson, F. J., & Sherwood, S. C. (2006), Modeling the impact of convective entrainment on
967 the tropical tropopause. *Journal of the Amotphseric Sciences*, *63*(3), 1013-1027.
968 https://doi.org/10.1175/JAS3673.1

969 Romps, D. M. (2011), Response of tropical precipitation to global warming. *Journal of the*
970 *Atmosphseric Sciences*, *68*(1), 123-138. https://doi.org/10.1175/2010JAS3542.1

971 Salby, M. & Callagha, P. (2004), Control of the tropical tropopause and vertical transport across
972 it. *Journal of Climate*, *17*(5), 965-985. https://doi.org/10.1175/1520-
973 0442(2004)017<0965:COTTTA>2.0CO;2

974 Santee, M. L., Manney, G. L., Livesey, N. J., Schwartz., M. J., Neu, J. L., & Read, W. G. (2017),
975 A comprehensive overview of the climatological composition of the Asian summer monsoon
976 anticyclone based on 10 years of Aura Microwave Limb Sounder measurements. *Jounral of*
977 *Geophysical Research: Atmospheres*, *122*(10), 5491-5514.
978 https://doi.org/10.1029/2016JD026408

979 Schneider, E. K., Kirtman, B. P. & Lindzen, R. S. (1999), Tropospheric water vapor and climate
980 sensitivity. *Journal of the Amotphseric Sciences*, *56*(11), 1649-1658.
981 https://doi.org/10.1175/1520-0469(1999)056<1649:TWVACS>2.0.CO;2

982 Schoeberl, M. R., Douglass, A. R., Stolarski, R. S., Pawson, S., Strahan, S. E., & Read, W.
983 (2008), Comparison of lower stratospheric tropical mean vertical velocities. *Journal of*
984 *Geophysical Research, 113*, D24109. https://doi.org/10.1029/2008JD010221

985 Schoeberl, M. R., & Dessler, A. E. (2011), Dehydration of the stratosphere. *Atmospheric*
986 *Chemistry and Physics*, *11*, 8433-8446, https://doi.org/10.5194/acp-11-8433-2011

987 Schoeberl, M. R., Dessler, A., & Wang, T. (2013), Modeling upper tropospheric and lower
988 stratospheric water vapor anomalies. *Atmospheric Chemistry and Physics*, *13*, 7783-7793,
989 https://doi.org/10.5194/acp-13-7783-2013

990 Schoeberl, M. R., Dessler, A., Wang, T., Avery, M., & Jensen, E. J. (2014), Cloud formation,
991 convection, and stratospheric dehydration. *Earth and Space Science*, *1*, 1-17,
992 https://doi.org/10.1002/2014EA000014

Schoeberl, M. R., Jensen, E. J., & Woods, S. (2015), Gravity waves amplify upper tropospheric dehydration by clouds. *Earth and Space Science*, *2*, 485-500. https://doi.org/10.1002/2015EA000127

Schoeberl, M. R., Dessler, A., Ye, H., Wang, T., Avery, M., & Jensen, E. (2016), The impact of gravity waves and cloud nucleation threshold on stratospheric water and tropical tropospheric cloud fraction. *Earth and Space Science*, *3*. https://doi.org/10.1002/2016EA000180

Schoeberl, M. R., Jensen, E. J., Podglajen, A., Coy, L., Candido, S., & Carver, R. (2017), Gravity wave spectra in the lower stratosphere diagnosed from project loon balloon trajectories. *Journal of Geophysical Research: Atmospheres, 122*, 88517-8524. https://doi.org/10.1002/2017JD026471

Schoeberl, M. R., Jensen, E. J., Pfister, L., Ueyama, R., Avery, M., & Dessler, A. (2018), Convective hydration of the upper troposphere and lower stratosphere. *Journal of Geophysical Research: Atmospheres, 123*, 4583-4593. https://doi.org/doi:10.1029/2018JD028286

Schoeberl, M. R., Jensen, E. J., Pfister, L., Ueyama, R., Wang, T., & Selkirk, H., et al. (2019), Water vapor, clouds, and saturation in the tropical tropopause layer. *Journal of Geophysical Research: Atmospheres, 124*, 3984-4003. https://doi.org/doi:10.1029/2018JD029849

Schwartz, M. J., Read, W. G., Santee, M. L., Livesey, N. J., Froidevaux, L., Lambert, A., et al. (2013), Convectively injected water vapor in the North American summer lowermost stratosphere. *Geophysical Research Letters*, *40*(10), 2316-2321. https://doi.org/10.1002/grl.50421

Selkirk, H. B. (1993), The tropopause cold trap in the Australian monsoon during STEP/AMEX 1987. *Journal of Geophysical Research: Atmospheres, 98*(D5), 8591-8610. https://doi.org/doi:10.1029/92JD02932

Sherwood, S. C., & Dessler, A. (2000), On the control of stratospheric humidity. *Geophysical Research Letters*, *27*(16), 2513-2516. https://doi.org/10.1029/2000GL011438

Sherwood, S. C., Horinouchi, T., & Zeleznik, H. A. (2003), Convective impact on temperatures observed near the tropical tropopause. *Journal of the Atmospheric Sciences*, *60*(15), 1847-1856. https://doi.org/10.1175/1520-0469(2003)060<1847:CIOTON>2.0.CO;2

Sherwood, S. C., Roca, R., Weckwerth, T. M., & Andronova, N. G. (2010), Tropospheric water vapor, convection, and climate. *Reviews of Geophysics*, *48*(2). doi:10.1029/2009rg000301

Smith, J. B., Wilmouth, D. M., Bedka, K. M., Bowman, K. P., Homeyer, C. R., Dykema, J. A., et al. (2017), A case study of convectively sourced water vapor observed in the overworld stratosphere over the United States. *Journal of Geophysical Research: Atmospheres, 122*(17), 9529-9554. https://doi.org/doi:10.1002/2017JD026831

Solomon, S., Rosenlof, K., Portmann, R., Daniel, J., Davis, S., Sanford, T., & Plattner, G.-K. (2010), Contributions of stratospheric water vapor changes to decadal variations in the rate of global warming. *Science*, *327*, 1219-1223.

Tan, J., Jakob, C., Rossow, W. B., & Tselioudis, G. (2015), Increases in tropical rainfall driven by changes in frequency of organized deep convection. *Nature*, *519*, 451-454. https://doi.org/10.1038/nature14339

Tegtemeier, S., Anstey, J., Davis, S., Dragani, R., Harada, Y., Ivanviu, I., et al. (2020), Temperature and tropopause characteristics from reanalyses data in the tropical tropopause layer. *Atmospheric Chemistry and Physics*, *20*, 753-770, https://doi.org/10.5194/acp-20-753-2020

Ueyama, R., Jensen, E. J., Pfister, L., Diskin, G. S., Bui, T. P., & Dean-Day, J. M. (2014), Dehydration in the tropical tropopause layer: A case study for model evaluation using aircraft observations. *Journal of Geophysical Research: Atmospheres, 119*, 5299-5316. https://doi.org/10.1002/2013JD021381

Ueyama, R., Jensen, E. J., Pfister, L., & Kim, J.-E. (2015), Dynamical, convective, and microphysical control on wintertime distributions of water vapor and clouds in the tropical tropopause layer. *Journal of Geophysical Research: Atmospheres, 120*, 10,483-10,500. https://doi.org/10.1002/2015JD023318

Ueyama, R., Jensen, E. J., & Pfister, L. (2018), Convective influence on the humidity and clouds in the tropical tropopause layer. *Journal of Geophysical Research: Atmospheres, 123*, 7576-7593. https://doi.org/10.1029/2018JD028674

Ueyama, R., Jensen, E. J., Pfister, L., Krämer, M., Afchine, A., & Schoeberl, M. (2020), Impact of convectively detrained ice crystals on the humidity of the tropical tropopause layer in boreal winter. *Journal of Geophysical Research: Atmospheres, 125*, e2020JD032894. https://doi.org/10.1029/2020JD032894

Virts, K., Wallace, J. M., Fu, Q., & Ackerman, T. P. (2010), Tropical tropopause transition layer cirrus as represented by CALIPSO lidar observations. *Journal of the Atmospheric Sciences*, *67*(10), 3097-3112. https://doi.org/10.1175/2010JAS3413.1

Wofsy, S. C., McConnell, J. C., & McElroy, M. B. (1972), Atmospheric $CH_4$, CO, and $CO_2$. *Journal of Geophysical Research, 77*(24), 4477-4493. https://doi.org/10.1029/JC077i024p04477

Yulaeva, E., Holton, J. R., & Wallace, J. M. (1994), On the cause of the annual cycle in tropical lower-stratospheric temperatures. *Journal of the Atmospheric Sciences*, *51*(2). https://doi.org/10.1175/1520-0469(1994)051<0169:OTCOTA>2.0.CO;2